crystals

MDPI

Review

Ferroelectricity in Simple Binary Crystals

Akira Onodera * and Masaki Takesada

Department of Physics, Faculty of Science, Hokkaido University, Sapporo 060-0810, Japan; mt@phys.sci.hokudai.ac.jp

* Correspondence: onodera@phys.sci.hokudai.ac.jp; Tel.: +81-11-706-2680

Academic Editor: Stevin Snellius Pramana

Received: 28 April 2017; Accepted: 23 May 2017; Published: 28 July 2017

Abstract: The origin of ferroelectricity in doped binary crystals, $Pb_{1-x}Ge_xTe$, $Cd_{1-x}Zn_xTe$, $Zn_{1-x}Li_xO$, and $Hf_{1-x}Zr_xO_2$ is discussed, while no binary ferroelectrics have been reported except for two crystals, HCl and HBr. The ferroelectricity is induced only in doped crystals, which shows an importance of electronic modification in chemical bonds by dopants. The phenomenological and microscopic treatments are given for the appearance of ferroelectric activity. The discovery of ferroelectricity in binary crystals such as ZnO and HfO_2 is of high interest in fundamental science and also in application for complementary metal–oxide semiconductor (CMOS) technology.

Keywords: ferroelectric; binary crystal; ZnO; HfO_2; mixed bond

1. Introduction

Ferroelectrics are expected as a key material for next-generation nonvolatile ferroelectric memories (FeRAM), piezoelectric actuators, high-*k* gate-materials for high-speed FET (field effect transistor), and optoelectronic devices [1–6]. Particularly, ferroelectric thin films such as perovskite PZT ($PbZr_{1-x}Ti_xO_3$) and Bi-layered perovskite SBT ($SrBi_2Ta_2O_9$) have been investigated extensively for FeRAM, because of their excellent dielectric properties, i.e., high dielectric constant and large spontaneous polarization. However, it is not so easy to fabricate good quality ferroelectric thin films on silicon substrate and integrate into devices overcoming degradation of ferroelectric properties due to the so-called size effect. Many ferroelectrics have crystal structures consisting of more than three atoms. For example, $BaTiO_3$, known as a typical ferroelectric with a perovskite structure, consists of three atoms. New materials with a simple structure are not only preferable for understanding the microscopic origin of ferroelectricity, but are also easy for integrating into modern ferroelectric devices. No ferroelectrics with two atoms have been reported except for two molecular crystals, HCl and HBr (Table 1) [7]. In 1969, Cochran developed the theory of lattice dynamics for alkali halide crystals such NaCl and discussed the possibility of ferroelectricity, which revealed a real alkali halide crystal is not a ferroelectric, because a short-range restoring contribution is about twice as great as a long-range Coulomb contribution as discussed later [8–10]. However, it is important to point out that these two contributions are the same order for alkali halide crystals. We will show in this article that this balance of these two contributions may be modified by introducing some dopants, strain or defects in crystals.

Table 1. Phase diagram of HCl and HBr after Hoshino et al. [7].

	Phase III Ferroelectric	Phase II Paraelectric			Phase I Liquid
HCl	Orthorhombic-$Bb2_1m$	Cubic-$Fm3m$			Liquid
	Below 98 K	98~159 K			Above 159 K
HBr	Orthorhombic-$Bb2_1m$	Phase IIc Orthorhombic-$Bbcm$	Phase IIb Cubic	Phase IIa Cubic-$Fm3m$	Liquid
	Below 90 K	90~114 K	114~117 K	117~186 K	Above 186 K

The electronic ferroelectricity was found in wide-gap semiconductor ZnO by introducing a small amount of Li dopants, although pure ZnO does not show any evidence of ferroelectricity [11–15]. ZnO has a simple binary AB structure with high-symmetry (wurtzite structure). Besides ZnO, Ge-doped PbTe, a IV-VI narrow-gap semiconductor [16], and Zn-doped CdTe, a II-VI wide-gap semiconductor [17], have been investigated as materials of binary crystals accompanying ferroelectricity (Figure 1). Moreover, recent works showed that thin films of HfO_2-ZrO_2 systems exhibit ferroelectricity [18,19]. Hafnia (HfO_2) and Zirconia (ZrO_2) have been well studied as high-k dielectric materials in CMOS (complementary metal–oxide semiconductor) technology. Pure HfO_2 crystal is monoclinic with space group $P2_1/c$ at room temperature and atmospheric pressure. Only HfO_2 thin films doped with Si, Y, Al and Zr change the monoclinic crystal structure to a polar orthorhombic structure. The discovery of ferroelectricity in binary crystals such as ZnO and HfO_2 is of high interest in fundamental science and also in application fields. Our concern is to study the origin of this unexpected appearance of ferroelectricity in doped binary crystals. We will discuss why the ferroelectricity does not appear in pure systems but in doped crystals.

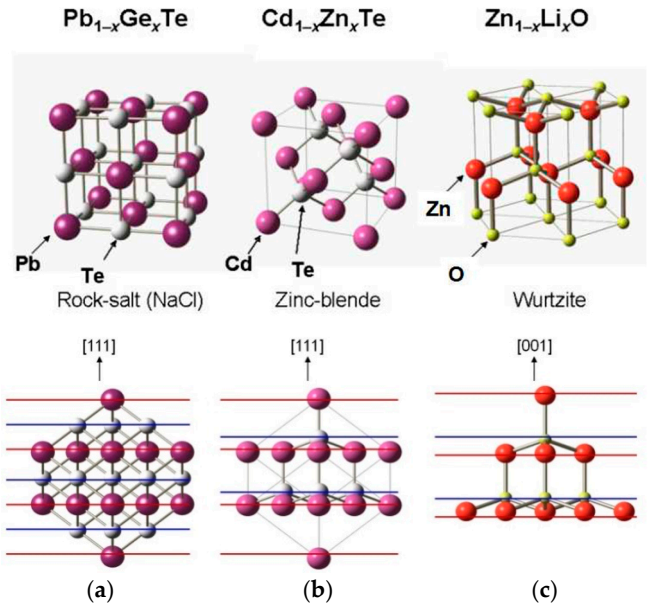

Figure 1. Crystal structures of (**a**) $Pb_{1-x}Ge_xTe$, (**b**) $Cd_{1-x}Zn_xTe$ and (**c**) $Zn_{1-x}Li_xO$. The lower figures are plots of cation (blue lines) and anion (red lines) layers along the polar rhombohedral [111] direction for $Pb_{1-x}Ge_xTe$ and $Cd_{1-x}Zn_xTe$, and polar [001] direction for $Zn_{1-x}Li_xO$ [15].

2. Ferroelectricity in Binary Semiconductors

Ferroelectrics, in general, have complicated crystal structures, which undergo a phase transition from a paraelectric high-temperature phase with decreasing temperature, breaking the symmetry of

inversion. The dielectric constant (ε) and the spontaneous polarization (P_s) are characterized in the mean field approximation as

$$\varepsilon = C/(T - T_c) \quad (1)$$

$$P_s = P_o\,(T - T_c)^{1/2} \quad (2)$$

where T_c is a critical temperature. Ferroelectrics are generally classified into order-disorder, displacive and improper types, though multiferroic materials have been reported recently. According to these types, they show the following characteristic dielectric properties as summarized in Table 2 [20].

Table 2. Typical values of the Curie-Weiss constant (C), the dielectric constant around T_c (ε_{max}), and the spontaneous polarization (P_s) according to the type of ferroelectrics.

Type of Ferroelectrics	C [K]	ε_{max} at T_c	P_s [μC/cm^2]	Example
Order-disorder	1~3 × 10^3	10^3	3~5	TGS [§]
Displacive	10^5	10^4	10~30	$BaTiO_3$
Improper	10	10	Small	ACS [#]
Electronic	-	21	0.9	ZnO

[§] TGS ($(NH_3CH_2COOH)_3H_2SO_4$), [#] ACS ($(NH_4)_2Cd_2(SO_4)_3$).

Binary ferroelectric crystals show different but common dielectric behavior from those of the usual ferroelectrics described above; a small dielectric anomaly at T_c and relatively large P_s. We will review the ferroelectric properties of the ferroelectric binary semiconductors, PbTe, CdTe and ZnO, and a high-k dielectric HfO_2, briefly in this section. More detailed discussion should be referred in a monograph [15].

2.1. Narrow-Gap Ferroelectric Semiconductor PbTe

The PbTe-GeTe system has been investigated extensively about its ferroelectricity among IV-VI semiconductors [16], which has a rock-salt type structure ($Fm3m$, a = 6.46 Å) at room temperature. The energy gap (E_g) is 0.3 eV, which is comparable to the Lorentz field $(4\pi/3)P$. The ferroelectricity is observed in solid solution $Pb_{1-x}Ge_xTe$. The stacking Pb^{2+} cation and Te^{2-} anion layers dimerize along the rhombohedral [111] direction, as shown in Figure 1. The crystal changes to a rhombohedral structure ($R3m$) which allows it to exhibit ferroelectric activity $Pb_{1-x}Ge_xTe$ with x = 0.003 shows a large dielectric anomaly at T = 100 K.

The large dielectric anomaly and the existence of the soft mode suggest the ferroelectric activity.

2.2. Wide-Gap Ferroelectric Semiconductor CdTe

$Cd_{1-x}Zn_xTe$ is a II-VI wide-gap semiconductor with E_g = 1.53 eV. Weil et al. discovered the ferroelectric activity in $Cd_{1-x}Zn_xTe$, as shown in Figure 2 [17,21]. The cubic zinc-blende structure (space group $F\overline{4}3m$, a = 6.486 Å) of pure CdTe crystal changes to a rhombohedral one ($R3m$, a = 6.401 Å, α = 89.94°) in $Cd_{1-x}Zn_xTe$, as shown in Figure 1b. The dielectric anomaly at T_c (393 K) is smaller by two orders than that of typical ferroelectric $BaTiO_3$ (~14,000). The spontaneous polarization is about 5 μC/cm^2 along the rhombohedral [111] direction. Doped Zn ions locate at *off-center* positions [22] which cause rhombohedral distortion of about 0.01 Å in $Cd_{1-x}Zn_xTe$ [22].

No soft mode has been observed in $Cd_{1-x}Zn_xTe$, and the dielectric anomaly is small. Although the behavior of *off-center ions* plays an important role in this ferroelectricity like $Pb_{1-x}Ge_xTe$, the occurrence of phase transition seems to be driven in a different way from that of $Pb_{1-x}Ge_xTe$.

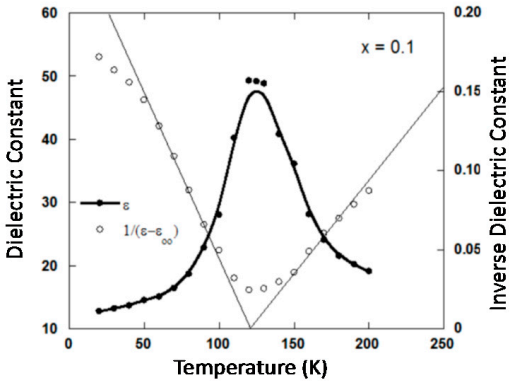

Figure 2. Dependence of dielectric constant and inverse dielectric constant in $Cd_{1-x}Zn_xTe$ (x = 0.1) on temperature [17]. Reprinted figure with permission from R. Weil, R. Nkum, E. Muranevich, and L. Benguigui, Physical Review Letters, 62, 2744, 1989. Copyright (1989) by the American Physical Society.

2.3. II-VI Wide-Gap Semiconductor ZnO

Zinc Oxide (ZnO), a II-VI wide-gap semiconductor, is a well-studied electronic material with a large piezoelectric constant [23–27]. ZnO has been studied as materials for solar cells, transparent conductors and blue lasers [28,29]. This crystal has a wurtzite structure ($P6_3mc$) (Figure 3). This space group is non-centrosymmetric and is allowed to exhibit ferroelectricity, although no *D-E* loop has been observed until melting point. Introduction of a small amount of Li-dopants results in the ferroelectricity.

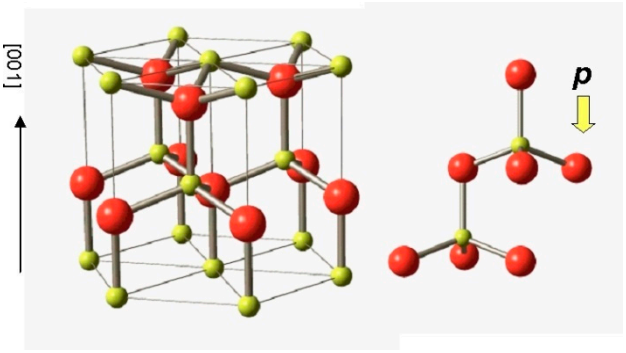

Figure 3. Crystal structure of ZnO. The observed polarization (p) is shown by a yellow arrow [15].

A dielectric anomaly in $Zn_{1-x}Li_xO$ (x = 0.09) was found at 470 K (T_c) (Figure 4), though pure ZnO shows no anomaly from 20 K to 700 K. The small dielectric anomaly (ε_{max} = 21) is the same order with $Cd_{1-x}Zn_xTe$ (ε_{max} = 50).

The spontaneous polarization is 0.9 $\mu C/cm^2$ [30,31]. The phase diagram between T_c and x is shown in Figure 5, which reminds us of a phase diagram of quantum ferroelectrics such as $KTa_{1-x}Nb_xO_3$ and $Sr_{1-x}Ca_xTiO_3$. Raman scattering measurements showed no soft modes [32,33].

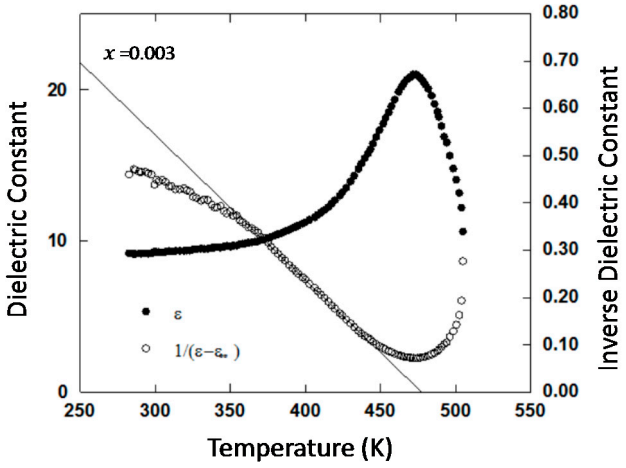

Figure 4. Temperature dependence of the dielectric constant of $Zn_{1-x}Li_xO$ (x = 0.09) [15].

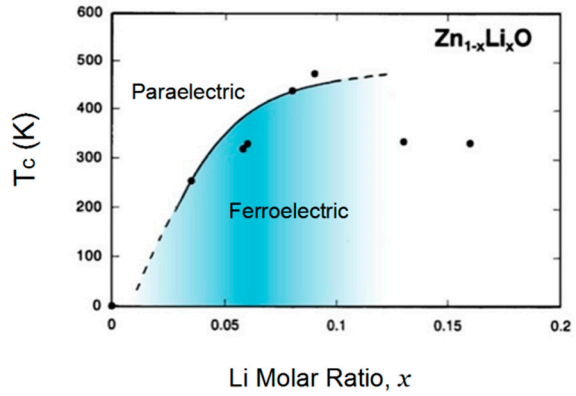

Figure 5. Phase diagram of the ferroelectric transition temperature (T_c) vs. Li molar ratio (x) in $Zn_{1-x}Li_xO$ [15].

2.4. High-k Materials HfO_2 and ZrO_2

HfO_2 and ZrO_2 are well-known high-temperature dielectrics. The thin films of HfO_2 and ZrO_2 have been studied extensively as a high-k gate dielectric film in CMOS technology. The crystal structure is monoclinic with space group $P2_1/c$ at room temperature and atmospheric pressure, which transforms to a tetragonal structure ($P4_2/nmc$) at ~1990 K, and then to a cubic Auorite structure ($Fm3m$) at ~2870 K. Other two orthorhombic phases have been reported under high pressure near 4 and 14 GPa [34]. Figure 6 shows a P-T phase diagram of HfO_2.

The monoclinic $P2_1/c$ structure is centrosymmetric, which does not show any ferroelectric activity. Thin films of HfO_2 undergo a phase transition to a noncentrosymmetric orthorhombic structure, breaking the symmetry of inversion when the films are doped with Si, Y, Al, or Zr [18,19,35–38]. The X-ray diffraction patterns of HfO_2, $Hf_{0.5}Zr_{0.5}O_2$ and ZrO_2 thin films are shown in Figure 7 [38]. Four space groups ($Pmn2_1$, $Pca2_1$, $Pbca$, and $Pbcm$) are proposed for this orthorhombic ferroelectric phase. Among these space groups, it is considered that $Pca2_1$ is the most probable. The sequence of phase transitions and crystal structures are shown in Figure 8. The ferroelectricity was confirmed by D-E hysteresis measurements, which revealed P_s of 16 μC/cm^2 as shown in Figure 9. The Curie temperature (T_c) was estimated to be about 623 K [39,40].

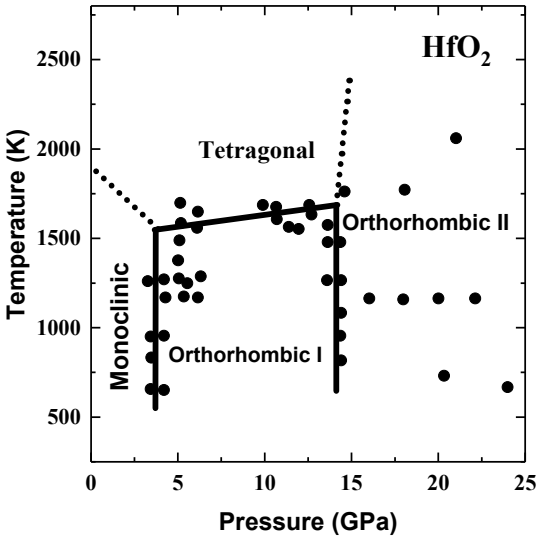

Figure 6. *P–T* phase diagram of HfO_2 [34].

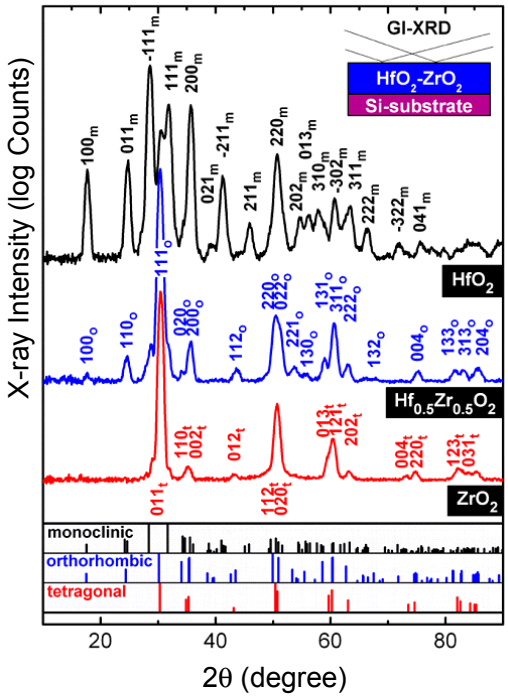

Figure 7. X-ray diffraction patterns of HfO_2, $Hf_{0.5}Zr_{0.5}O_2$ and ZrO_2 thin films on silicon substrates. The Bragg reflections are assigned as *h k l* with suffixes *m*, *o* and *t*, which indicate monoclinic, orthorhombic and tetragonal lattices, respectively [38]. Reprinted with permission from Johannes Müller, Tim S. Böscke, Uwe Schröder, et al., Ferroelectricity in Simple Binary ZrO_2 and HfO_2, Nano Letters, 2012, 12, 4318–4323. Copyright (2012) American Chemical Society.

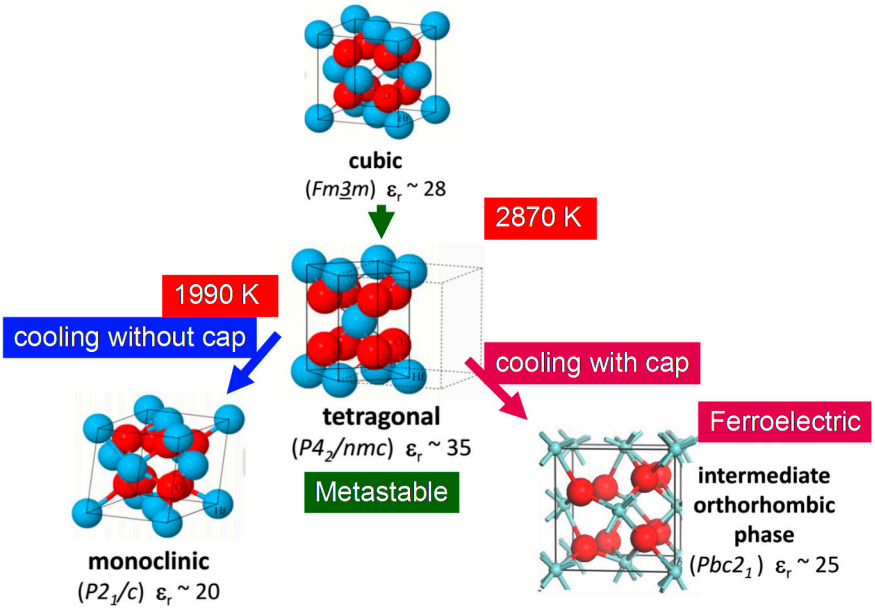

Figure 8. Sequence of phase transitions and crystal structures of HfO_2.

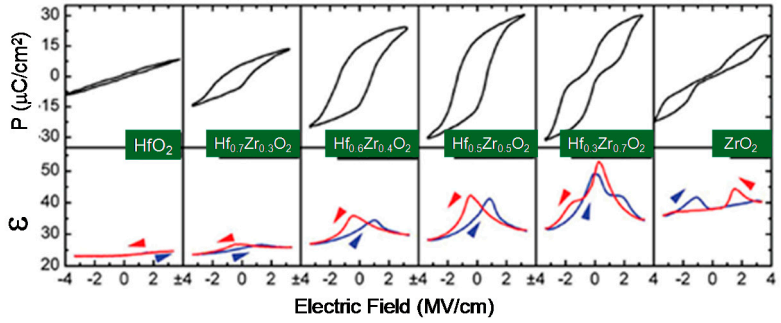

Figure 9. *P-E* hysteresis loops and dielectric constant (ε) in thin films of HfO_2-ZrO_2 system [38]. Reprinted with permission from Johannes Müller, Tim S. Böscke, Uwe Schröder, et al., Ferroelectricity in Simple Binary ZrO_2 and HfO_2, Nano Letters, 2012, 12, 4318–4323. Copyright (2012) American Chemical Society.

3. Phenomenological Treatment for the Appearance of Ferroelectricity

Firstly following the Landau theory, we consider the free energy (F) for the paraelectric phase of binary crystals in terms of polarization P as

$$F = 1/2\alpha P^2 + 1/4\beta P^4 + \dots , \quad (3)$$

where α, and β are coefficients. In general, the only coefficient α depends on temperature as

$$\alpha = \alpha_o\,(T - T_o),\ \alpha_o > 0 \quad (4)$$

In the case for paraelectric dielectrics, the critical temperature T_o is considered to be lower than 0 K, because of the absence of phase transitions above 0 K. When some dopants are introduced to crystals, some structural changes due to a difference in atomic radii and bonding electrons are modified

by dopants. These may induce some local changes in electronic distribution in crystals. These extra contributions could be added to the above free energy as

$$F = 1/2\alpha P^2 + 1/4\beta P^4 + g\eta P + 1/2\alpha'\eta^2 \ldots , \quad (5)$$

where the last term $1/2\alpha'\eta^2$ is the contribution by dopants, and $g\eta P$ is an interaction term between the host crystal and extrinsic dopants. From the stability condition $\partial F/\partial\eta = 0$,

$$\eta = -(g/\alpha')P, \quad (6)$$

The above free energy F can be rewritten as

$$F = 1/2(\alpha - g^2/\alpha')P^2 + 1/4\beta P^4 \quad (7)$$

Using Equation (4), we get

$$(\alpha - g^2/\alpha') = \alpha_0 (T - T_c) \quad (8)$$

where

$$T_c = T_o + g^2/\alpha_0\alpha' \quad (9)$$

As the critical temperature T_c increases when the coefficient α' is positive, it should be possible to undergo a ferroelectric phase transition. T_c shows a rapid increase in the order of 10^2 K for large g and small α' in the case of $Pb_{1-x}Ge_xTe$, $Cd_{1-x}Zn_xTe$, and $Zn_{1-x}Li_xO$. The appearance of ferroelectricity is realized in the doped binary crystals, while any phase transition does not occur in pure crystals.

4. Microscopic Consideration after Cochran's Lattice Dynamical Theory

Although the above phenomenological theory can explain well the appearance of ferroelectricity, it is not so easy for us to understand what kind of phenomena occurs in real crystals. For binary crystals such as NaCl, Cochran proposed a lattice dynamical theory to elucidate the origin of ferroelectric phase transition based on the shell model [9,10]. We review simply Cochran's soft mode theory for ferroelectrics at first.

Cochran calculated the frequencies of transverse and optic phonon modes in a diatomic cubic crystal using a shell model such as NaCl, as illustrated in Figure 10. The shell is originated from some local lattice deformation, electronic overlap forces, or covalency in chemical bonds. The core of the negative ion (charge *Xe*, mass m_2) will interact through an outer shell (charge *Ye*, mass ~0) with a force constant *k*. The positive ion (charge *Ze*, mass m_1) interacts with the shell by a short range force through a force constant R_o. The displacements are denoted as u_1, v_2 and u_2 for the positive ion, shell and negative core, respectively.

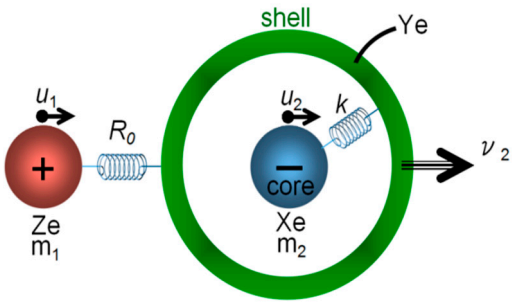

Figure 10. Schematic diagram of a shell model for a diatomic crystal.

The frequencies of the transverse and longitudinal optic modes, ω_{TO} and ω_{LO} are calculated as

$$\mu\omega_{TO}{}^2 = R_o' - \frac{4\pi(\varepsilon_\infty + 2)(Z'e)^2}{9V} \tag{10}$$

$$\mu\omega_{LO}{}^2 = R_o' + \frac{8\pi(\varepsilon_\infty + 2)(Z'e)^2}{9V\varepsilon_\infty} \tag{11}$$

where

$$R_o' = \frac{kR_o}{k + R_o} < R_o \tag{12}$$

$$Z' = Z + \frac{YR_o}{k + R_o} < Z \tag{13}$$

$$\mu = \frac{m_1 m_2}{m_1 + m_2} \tag{14}$$

ε_∞ and V are a high-frequency dielectric constant and the unit cell volume. Following the Lyddane-Sachs-Teller (LST) relation, the dielectric constant ε is given as

$$\frac{\varepsilon}{\varepsilon_\infty} = \frac{\omega_{LO}{}^2}{\omega_{TO}{}^2} \tag{15}$$

The ferroelectric phase is realized if ω_{TO} = 0 in Equation (10), because ferroelectric phase transitions generally accompany with a divergence of dielectric constant. The ferroelectricity is induced from the delicate balance between the short-range term R_o' and the second dipolar Coulomb term in the right side of Equation (10).

Cochran showed that a real alkali halide crystal is not a ferroelectric, because R_o' is about twice as great as the other while these two contributions are the same order for real alkali halide crystals. This is one reason why the ferroelectricity has been found only in HCl and HBr. Dopants will change local electronic distribution of chemical bond, i.e., the nature of covalency, particularly in mixed bonded crystals. Dopants also force it to displace to *off-centered* positions and induce local structural distortions. Particularly, the chemical bonds may be affected sensitively by dopants in ZnO, CdTe and HfO_2 where the degree of covalency (or iconicity) is nearly half, as shown in Table 3. The balance between the restoring force R_o' and the dipolar Coulomb force can be modified by dopants, defects or strain.

Table 3. Dielectric constant and fractional degree of iconicity after J.C. Phillips, Bonds and Bands in Semiconductors [41].

Materials	ε at R.T.	Fractional Degree of Ionicity
NaCl	5.6	0.94
MgO	10.0	0.84
ZnO	8.8	0.62
CdTe	7.1	0.67
HfO_2	25	0.8
ZrO_2	30~46	0.8
TiO_2	170	0.6
Si	3.6	0

5. Discussion

5.1. Electronic Ferroelectricity in ZnO; Effect of Dopants

The replacement of host Zn ions by substitutional Li ions plays a primary role for the appearance of ferroelectricity in ZnO. To clarify the effect of dopants, structural size-mismatch and electronic models are studied: the introduction of small Be^{2+} ions (ionic radius 0.3 Å) should be effective than

Li^+ (ionic radius 0.6 Å) and Mg^{2+} (ionic radius 0.65 Å) ions if the ionic size-mismatch is important for ferroelectricity, while Mg^{2+} ions ($1s^2 2s^2 2p^6$) should play a different role from the isoelectronic Li^+ and Be^{2+} ions ($1\ s^2$) if the electronic configuration is important.

The series of dielectric measurements show that the introduction of Mg^{2+} ions suppresses T_c [42]. The appearance of ferroelectricity is primarily due to electronic origin.

5.2. Structural Modification by Dopants

The electronic distribution, especially the nature of *d-p* hybridization of paraelectric pure ZnO and ferroelectric $Zn_{1-x}Li_xO$ at 19 K, was measured directly by X-ray diffraction. The main difference is observed in electronic distribution around Zn ion, as shown in Figure 11.

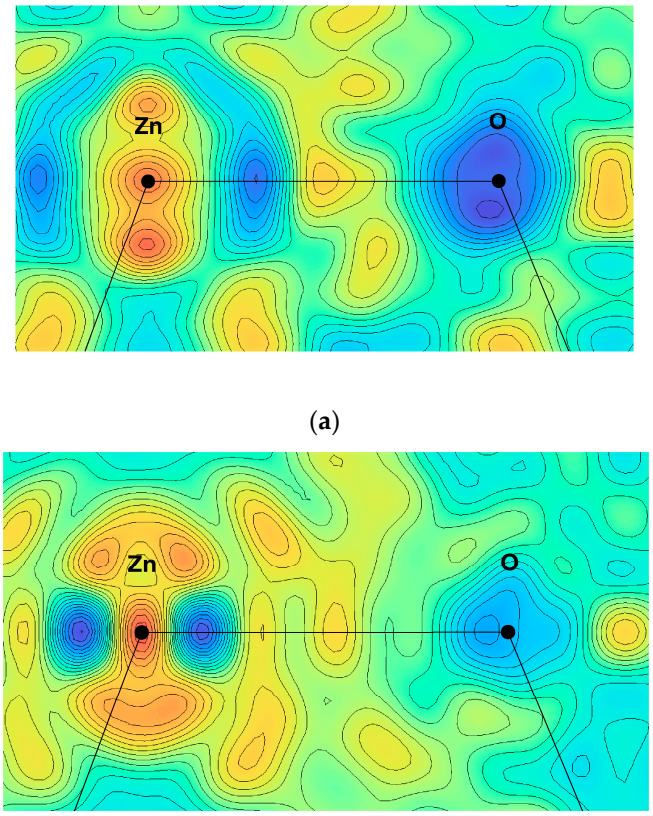

Figure 11. The difference Fourier maps of (**a**) paraelectric ZnO and (**b**) ferroelectric $Zn_{1-x}Li_xO$ at 19 K in the (110) plane with a contour increment of 0.2 $e/Å^3$. The horizontal straight lines from Zn to O ions are the [001] direction. Bluish cold color means negative charge density and reddish warm region is positive charge density.

The negative distribution is observed around the Zn atom in $Zn_{1-x}Li_xO$, whose shape corresponds to Zn-$3d_z{}^2$-orbital. This evidence shows that the Zn 3*d*-electrons disappear around Zn position in the doped ZnO.

Most crystals have a fraction of covalent and ionic bonding components. ZnO is bonded half by ionic and half by covalent forces, of which delicate balance is slightly changed by Li-dopants without *d-electrons*. Pure ZnO has large dipole moment [11], while this host dipole could not be reversible by an electric field. In $Zn_{1-x}Li_xO$, the dipole is reduced a little bit by the local electronic deformation along the polar (0 0 1) direction; this is, in other words, an introduction of *negative dipoles* in the host lattice. These *negative dipoles* are responsible for an electric field and behave as "*hole dipoles*" which are

similar to "*hole electrons*" in *n*-type semiconductors. We should call this type of ferroelectrics as "*n-type ferroelectrics*", while usual ferroelectrics are "*p-type ferroelectrics*".

In the case of $Hf_{1-x}Zr_xO_2$, the ionic radii (0.83 Å for Hf^{4+} and 0.84 Å for Zr^{4+}) are almost the same. The main difference is an electronic structure, Hf ($-4f^{14}$) and Zr ($-4p^6$). As the high dielectric constants in these crystals (ε = 25 for HfO_2, ε = 30~46 for ZrO_2) mean the large splitting of ω_{TO} and ω_{LO} phonon modes, a ω_{TO} phonon mode is much lower compared with a ω_{LO} (LST relation, Equation (10)). In this sense, HfO_2 and ZrO_2 are incipient ferroelectrics as $SrTiO_3$. The electronic distribution in the Hf-O bond is perturbed by Zr dopants without *f*-electrons. This modification may stabilize an orthorhombic polar structure and results in the appearance of ferroelectricity in $Hf_{1-x}Zr_xO_2$.

The above microscopic consideration gives us one perspective to understand the origin of ferroelectricity in doped binary crystals. If the condition that ω_{TO} approaches to zero at T_c holds exactly, soft mode should be detectable. However, no soft mode has been observed in $Cd_{1-x}Zn_xTe$, $Zn_{1-x}Li_xO$ and $Hf_{1-x}Zr_xO_2$, except for $Pb_{1-x}Ge_xTe$. This evidence suggests that the mechanism of the ferroelectric phase transition is not so simple in real crystals which are partially covalent and partially ionic. The small dielectric anomaly in $Cd_{1-x}Zn_xTe$, $Zn_{1-x}Li_xO$ and $Hf_{1-x}Zr_xO_2$ reminds us of an improper type ferroelectrics, rather than the order-disorder-type and displacive-type of ferroelectrics. This problem has been left for our future studies.

6. Another Possible Ferroelectric TiO_2

Rutile TiO_2 is studied well by various techniques [43]. The structure is tetragonal with space group $P4_2/mnm$ (a = 4.593659 (18) and c = 2.958682 (8) Å at 298 K, Z = 2) (Figure 12) [44]. Besides rutile, TiO_2 admits another two polymorphic forms in nature, i.e., anatase ($I4_1/amd$, a = 3.7845, c = 9.5143 Å, Z = 4) and brookite ($Pbca$, a = 5.4558, b = 9.1819, c = 5.1429 Å, Z = 8). Rutile TiO_2 is the most common of the three polymorphic forms. Under high pressure, TiO_2 undergoes a series of structural phase transitions.

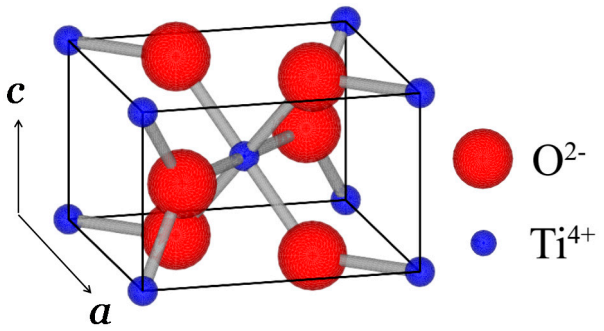

Figure 12. Crystal structure of Rutile TiO_2. Ti (blue) and O (red).

Rutile TiO_2 has large refractive indices (n_c = 2.903, n_a = 2.616) and large static dielectric constants (ε_c = 170, ε_a = 86) at room temperature.

Parker measured the dielectric constant ε of TiO_2 which increases with decreasing temperature, but does not show any anomaly from 1.6 to 1060 K, as shown in Figure 13 [45,46]. Pure TiO_2 does not show any ferroelectric or antiferroelectric activity. The dielectric constant shows a plateau at low temperatures around 0 K, which reminds us of dielectric behavior in quantum paraelectrics, such as $SrTiO_3$.

Although there had been a long-running discussion concerning the covalency of the bonding in rutile, Gronschorek [47] and Sakata et al. [48] concluded that Ti-O bonding in rutile is largely covalent, as shown in Figure 14. If we can modify the nature of bonding by some dopants or stress, it may be possible to expect the appearance of ferroelectricity.

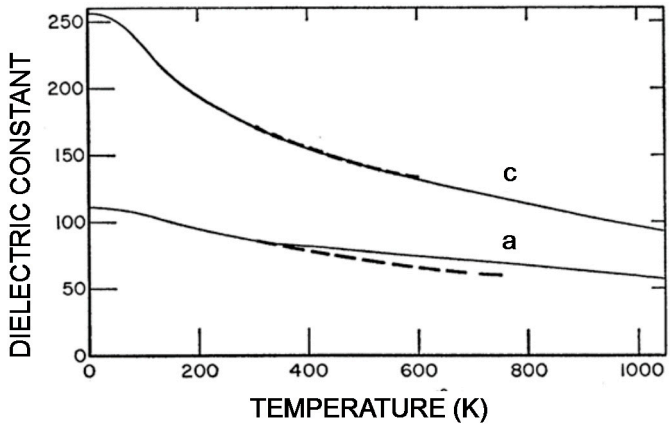

Figure 13. Temperature dependence of dielectric constant of rutile TiO_2 along the *a*- and *c*-directions. The solid lines are after Parker [45] and the dashed lines after von Hippel [46].

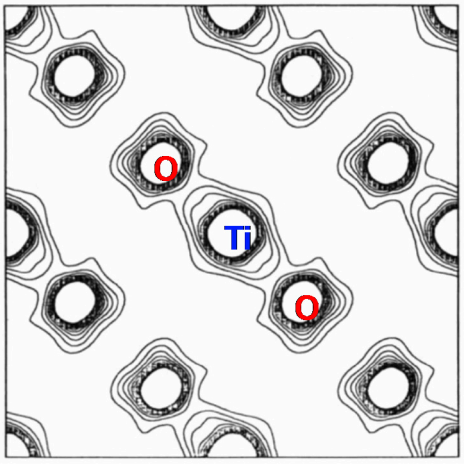

Figure 14. Electron density map of rutile TiO_2 on the (0 0 2) plane. Charge of 0.4 e $Å^{-3}$ is observed in Ti-O bond.

Recently, Montanari and Harrison proposed by density functional calculations that ferroelectric instability can be possible in rutile TiO_2 by applying a negative isotropic pressure [49]. The TO A2*u* mode, which is the *c*-axis ferroelectric mode, vanishes at -4 GPa, thereby leading to a crystal instability.

Similar calculations on binary oxides such BaO, CaO, MgO, EuO, SnO_2 have been reported recently [50,51], although these crystals are primarily ionic (the degree of ionicity is ~0.8). They showed that ferroelectricity can be induced even in simple alkaline-earth-metal binary oxides by using appropriate epitaxial strains in thin films or in nano-particles.

7. Conclusions

We discussed the origin of ferroelectricity in doped binary crystals, $Pb_{1-x}Ge_xTe$, $Cd_{1-x}Zn_xTe$, $Zn_{1-x}Li_xO$, and $Hf_{1-x}Zr_xO_2$ on the basis of phenomenological and lattice dynamical treatments, while no ferroelectrics have been reported in pure binary crystals except for HCl and HBr. The delicate balance of the short-range restoring force and the long-range dipolar Coulomb force is tuned by dopants, particularly in binary crystals which are half covalent and half ionic. The modification of the electronic distribution in the chemical bond results in the local structural distortion, which may stabilize a non-centrosymmetric polar structure from a paraelectric structure with high-symmetry.

The discovery of ferroelectricity in doped binary crystals shows us a richness of structural science. Moreover, the ferroelectric HfO_2 is expected to be a promising candidate for FeRAM and high-speed

FET. Ferroelectrics are a group of materials sensitive to small structural changes. We must take into account the electronic contribution in the case of simple binary crystals discussed here. Further precise structural and theoretical studies should be necessary to clarify the possibility of ferroelectricity in other doped binary crystals.

Acknowledgments: This work was partially supported by Grant-in-Aid for Scientific Research (C) from JSPS No. 26400306 and a research granted from The Murata Science Foundation.

Conflicts of Interest: The authors declare no conflict of interest.

References

1. Auciello, O.; Scott, J.F.; Ramesh, R. Ultrahigh-Intensity Lasers: Physics of the Extreme on a Tabletop. *Phys. Today* **1998**, *51*, 22. [CrossRef]
2. Scott, J.F. The physics of ferroelectric ceramic thin films for memory applications. *Ferroelectr. Rev.* **1998**, *1*, 1. [CrossRef]
3. Haertling, G.H. Ferroelectric Ceramics: History and Technology. *J. Am. Ceram. Soc.* **1999**, *82*, 797–818. [CrossRef]
4. Scott, J.F.; Paz de Araujo, C.A. Ferroelectric memories. *Science* **1989**, *246*, 1400–1405. [CrossRef] [PubMed]
5. Uchino, K. Ceramic actuators: Principles and applications. *MRS Bull.* **1993**, *18*, 42–48. [CrossRef]
6. Wemple, S.H.; DiDomenico, M., Jr. Oxygen-Octahedra Ferroelectrics. II. Electro-optical and Nonlinear-Optical Device Applications. *J. Appl. Phys.* **1969**, *40*, 735. [CrossRef]
7. Hoshino, S.; Shimaoka, S.; Niimura, K. Ferroelectricity in Solid Hydrogen Halides. *Phys. Rev. Lett.* **1967**, *19*, 1286. [CrossRef]
8. Cochran, W. Crystal Stability and the Theory of Ferroelectricity. *Phys. Rev. Lett.* **1959**, *3*, 412. [CrossRef]
9. Cochran, W. Crystal stability and the theory of ferroelectricity. *Adv. Phys.* **1960**, *9*, 387. [CrossRef]
10. Cochran, W. Crystal stability and the theory of ferroelectricity part II. Piezoelectric crystals. *Adv. Phys.* **1961**, *10*, 401. [CrossRef]
11. Corso, D.A.; Posternak, M.; Resta, R.; Baldereshi, A. Ab initio study of piezoelectricity and spontaneous polarization in ZnO. *Phys. Rev.* **1994**, *B50*, 10715. [CrossRef]
12. Tamaki, N.; Onodera, A.; Sawada, T.; Yamashita, H. Measurements of D-E Hysteresis Loop and Ferroelectric Activity in Piezoelectric Li-doped ZnO. *J. Korean Phys.* **1996**, *29*, 668.
13. Onodera, A.; Tamaki, N.; Kawamura, Y.; Sawada, T.; Yamashita, H. Dielectric Activity and Ferroelectricity in Piezoelectric Semiconductor Li-Doped ZnO. *Jpn. J. Appl. Phys.* **1996**, *35*, 5160. [CrossRef]
14. Onodera, A.; Tamaki, N.; Jin, K.; Yamashita, H. Ferroelectric Properties in Piezoelectric Semiconductor $Zn_{1-x}M_xO$ (M=Li, Mg). *Jpn. J. Appl. Phys.* **1997**, *36*, 6008. [CrossRef]
15. Onodera, A.; Takesada, M. Electronic Ferroelectricity in II-VI Semiconductor ZnO. In *Advances in Ferroelectrics*; INTECH: Rijeka, Croatia, 2012.
16. Bilz, H.; Bussmann-Holder, A.; Jantsch, W.; Vogel, P. *Dynamical Properties of IV-VI Compounds*; Springer: Berlin, Germany, 1983.
17. Weil, R.; Nkum, R.; Muranevich, E.; Benguigui, L. Ferroelectricity in zinc cadmium telluride. *Phys. Rev. Lett.* **1989**, *62*, 2744. [CrossRef] [PubMed]
18. Böscke, T.S.; Müller, J.; Brauhaus, D.; Schröder, U.; Böttger, U. Ferroelectricity in hafnium oxide thin films. *Appl. Phys. Lett.* **2011**, *99*, 102903. [CrossRef]
19. Böscke, T.S.; Teichert, S.; Brauhaus, D.; Müller, J.; Schröder, U.; Böttger, U.; Mikolajick, T. Phase transitions in ferroelectric silicon doped hafnium oxide. *Appl. Phys. Lett.* **2011**, *99*, 112904. [CrossRef]
20. Mitsui, T.; Tatsuzaki, I.; Nakamura, E. *An Introduction to the Physics of Ferroelectrics*; Gordon and Breach: New York, NY, USA, 1976; p. 202.
21. Benguigui, L.; Weil, R.; Muranevich, E.; Chack, A.; Fredj, E. Ferroelectric properties of $Cd_{1-x}ZnxTe$ solid solutions. *J. Appl. Phys.* **1993**, *74*, 513. [CrossRef]
22. Terauchi, H.; Yoneda, Y.; Kasatani, H.; Sakaue, K.; Koshiba, T.; Murakami, S.; Kuroiwa, Y.; Noda, Y.; Sugai, S.; Nakashima, S.; et al. Ferroelectric behaviors in semiconductive $Cd_{1-x}ZnxTe$ crystals. *Jpn. J. Appl. Phys.* **1993**, *32*, 728. [CrossRef]

23. Klingshirn, C.F.; Meyer, B.K.; Waag, A.; Hoffmann, A.; Geurts, J. *Zinc Oxide From Fundamental Properties Towards Novel Applications*; Springer: Berlin, Germany, 2010.
24. Yao, T. (Ed.) *ZnO Its Most Up-to-Date Technology and Application, Perspectives*; CMC Books: Tokyo, Japan, 2007. (In Japanese)
25. Heiland, G.; Mollwo, E.; Stockmann, F. Electronic Processes in Zinc Oxide. *Solid State Phys.* **1959**, *8*, 191–323. [CrossRef]
26. Campbell, C. *Surface Acoustic Wave Devices and Their Signal Processing Application*; Academic Press: San Diego, CA, USA, 1989.
27. Hirshwald, W.; Bonasewicz, P.; Ernst, L.; Grade, M.; Hofmann, D.; Krebs, S.; Littbarski, R.; Neumann, G.; Grunze, M.; Kolb, D.; et al. *Current Topics in Materials Science*; Kaldis, E., Ed.; North-Holland: Amsterdam, The Netherlands, 1981; Volume 7, p. 148.
28. Tsukazaki, A.; Ohtomo, A.; Onuma, T.; Ohtani, M.; Makino, T.; Sumiya, M.; Ohtani, K.; Chichibu, S.F.; Fuke, S.; Segawa, Y.; et al. Repeated temperature modulation epitaxy for p-type doping and light-emitting diode based on ZnO. *Nat. Mater.* **2005**, *4*, 42–46. [CrossRef]
29. Joseph, M.; Tabata, H.; Kawai, T. p-Type Electrical Conduction in ZnO Thin Films by Ga and N Codoping. *Jpn. J. Appl. Phys.* **1999**, *38*, L1205. [CrossRef]
30. Onodera, A.; Yoshio, K.; Satoh, H.; Yamashita, H.; Sakagami, N. Li-Substitution Effect and Ferroelectric Properties in Piezoelectric Semiconductor ZnO. *Jpn. J. Appl. Phys.* **1998**, *37*, 5315. [CrossRef]
31. Onodera, A.; Tamaki, N.; Satoh, H.; Yamashita, H.; Sakai, A. Novel ferroelectricity in piezoelectric ZnO by Li-substitution. In *Dielectric Ceramic Materials: Ceramic Transactions*; Nair, K.M., Bhalla, A.S., Eds.; American Ceramic Society: Westerville, OH, USA, 1999; Volume 100, pp. 77–94.
32. Islam, E.; Sakai, A.; Onodera, A. Optical Phonons in Ferroelectric-Semiconductor Zn 0.8Li 0.2O Single Crystal Studied by Micro-Raman Scattering. *J. Phys. Soc. Jpn.* **2001**, *70*, 576. [CrossRef]
33. Kagami, D.; Takesada, M.; Onodera, A.; Satoh, H. Photoinduced Effect in Li-doped ZnO studied by Raman Scattering. *J. Korean Phys.* **2011**, *59*, 2532. [CrossRef]
34. Ohtaka, O.; Fukui, H.; Kunisada, T.; Fujisawa, T.; Funakoshi, K.; Utsumi, W.; Irifune, T.; Kuroda, K.; Kikegawa, T. Phase relations and volume changes of hafnia under high pressure and high temperature. *J. Am. Ceram. Soc.* **2001**, *84*, 1369–1373. [CrossRef]
35. Müller, J.; Schröder, U.; Böscke, T.S.; Müller, I.; Böttger, U.; Wilde, L.; Sundqvist, J.; Lemberger, M.; Kücher, P.; Mikolajick, T.; et al. Ferroelectricity in yttrium-doped hafnium oxide. *J. Appl. Phys.* **2011**, *110*, 114113. [CrossRef]
36. Müller, S.; Müller, J.; Singh, A.; Riedel, S.; Sundqvist, J.; Schröder, U.; Mikolajick, T. Incipient Ferroelectricity in Al-Doped HfO_2 Thin Films. *Adv. Funct. Mater.* **2012**, *22*, 2412–2417. [CrossRef]
37. Müller, J.; Böscke, T.S.; Brauhaus, D.; Schröder, U.; Böttger, U.; Sundqvist, J.; Kücher, P.; Mikolajick, T.; Frey, L. Ferroelectric $Zr_{0.5}Hf_{0.5}O_2$ thin films for nonvolatile memory applications. *Appl. Phys. Lett.* **2011**, *99*, 112901. [CrossRef]
38. Müller, J.; Böscke, T.S.; Schröder, U.; Müller, S.; Brauhaus, D.; Böttger, U.; Frey, L.; Mikolajick, T. Ferroelectricity in Simple Binary ZrO_2 and HfO_2. *Nano Lett.* **2012**, *12*, 4318–4323. [CrossRef] [PubMed]
39. Shimizu, T.; Katayama, K.; Kiguchi, T.; Akama, A.; Konno, J.; Sakata, O.; Funakubo, H. The demonstration of significant ferroelectricity in epitaxial Y-doped HfO_2 film. *Sci. Rep.* **2016**, *6*, 32931. [CrossRef] [PubMed]
40. Shimizu, T.; Katayama, K.; Kiguchi, T.; Akama, A.; Konno, T.J.; Hiroshi Funakubo, H. Growth of epitaxial orthorhombic YO1.5-substituted HfO2 thin film. *Appl. Phys. Lett.* **2015**, *107*, 032910. [CrossRef]
41. Phillips, J.C. *Bonds and Bands in Semiconductors*; Academic Press: New York, NY, USA, 1973.
42. Hagino, S.; Yoshio, K.; Yamazaki, T.; Satoh, H.; Matsuki, K.; Onodera, A. Electronic ferroelectricity in ZnO. *Ferroelectrics* **2001**, *264*, 235. [CrossRef]
43. Grants, F.A. Properties of Rutile (Titanium Dioxide). *Rev. Mod. Phys.* **1959**, *31*, 646–674. [CrossRef]
44. Abrahams, S.C.; Bernstein, J.L. Rutile: Normal Probability Plot Analysis and Accurate Measurement of Crystal Structure. *J. Chem. Phys.* **1971**, *55*, 3206–3211. [CrossRef]
45. Parker, R.A. Static Dielectric Constant of Rutile (TiO2), 1.6–1060°K. *Phys. Rev* **1961**, *124*, 1719. [CrossRef]
46. Von Hippel, A.R. *Dielectric Materials and Applications*; John Wiley & Sons: New York, NY, USA, 1954.
47. Gronschorek, W. X-ray charge density study of rutile (TiO_2). *Z. Kristallogr.* **1982**, *160*, 187–203. [CrossRef]
48. Sakata, M.; Uno, T.; Takata, M.; Mori, R. Electron Density in Rutile (TiO_2) by the Maximum Entropy Method. *Acta Crystallogr.* **1992**, *B48*, 591–598. [CrossRef]

49. Montanari, B.; Harrison, N.M. Pressure-induced instabilities in bulk TiO_2 rutile. *J. Phys. Condens. Matter* **2004**, *16*, 273. [CrossRef]
50. Bousquet, E.; Spaldin, N.A.; Ghosez, P. Strain-Induced Ferroelectricity in Simple Rocksalt Binary Oxides. *Phys. Rev. Lett.* **2010**, *104*, 037601. [CrossRef] [PubMed]
51. Glinchuk, M.D.; Khist, V.; Eliseev, E.A.; Morozovska, A.N. Ferroic properties of nanosized SnO_2. *Phase Transit.* **2013**, *86*, 903–909. [CrossRef]

© 2017 by the authors. Licensee MDPI, Basel, Switzerland. This article is an open access article distributed under the terms and conditions of the Creative Commons Attribution (CC BY) license (http://creativecommons.org/licenses/by/4.0/).